IEEE Photonics Journal
An IEEE Photonics Society Publication

Open Access

Multiple Fano Resonances Based on End-Coupled Semi-Ring Rectangular Resonator

Volume 11, Number 4, August 2019

Yihong Fang
Kunhua Wen
Zhengfeng Li
Bingye Wu
Li Chen
Jinyun Zhou
Dongyue Zhou

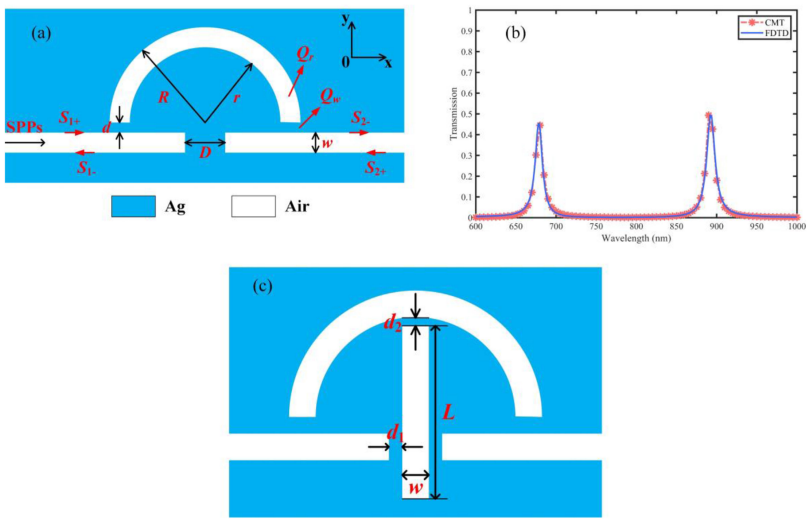

DOI: 10.1109/JPHOT.2019.2914483
1943-0655

Multiple Fano Resonances Based on End-Coupled Semi-Ring Rectangular Resonator

Yihong Fang, Kunhua Wen, Zhengfeng Li, Bingye Wu, Li Chen, Jinyun Zhou, and Dongyue Zhou

School of Physics and Optoelectronic Engineering, Guangdong University of Technology, Guangzhou 510006, China

DOI:10.1109/JPHOT.2019.2914483

Manuscript received March 9, 2019; revised April 23, 2019; accepted April 29, 2019. Date of publication May 2, 2019; date of current version June 26, 2019. This work was supported in part by Science and Technology Project of Guangzhou (201904010243), in part by Science and Technology Planning Projects of Guangdong Province, China (2016A020223013), in part by Science and Technology Major Projects of Guangdong Province (2018B010114002), in part by the National Natural Science Foundation of China (61475037), in part by the Natural Science Foundation of Guangdong Province, China (2014A030310300), in part by the State Key Lab of Optical Technologies for Micro-Engineering and Nano-Fabrication of China, and in part by the Foundation for Distinguished Young Talents in Higher Education of Guangdong, China (2014KQNCX066). Corresponding author: Kunhua Wen (e-mail: khwen@gdut.edu.cn).

Abstract: In this paper, multiple Fano resonances based on semi-ring-rectangular composite cavity (SRRCC) structure are numerically investigated and explained by the finite-difference time-domain method and the multiple interference coupled mode theory method. High refractive-index sensitivities and high figure of merits (FOMs) are obtained in SRRCC system, and thus it may be preferred in the chip-scale optical sensing area. Besides, the phase response and the delay time within the Fano resonant windows are also investigated. Additionally, two more Fano resonances with high sensitivities and FOMs emerge through adding a new semi-ring cavity. These structures show widely applications in the sensing area and promote development of on-chip integrated photonics.

Index Terms: Fano resonances, semi-ring-rectangular composite cavity (SRRCC), chip-scale optical sensing.

1. Introduction

Fano resonance, which is caused by the coherent interaction between a discrete state and a continuous one, has played an important role in the plasmonic researches over recent years [1]–[6]. Compared with Fabry–Pérot (FP) resonance, sharp asymmetrical spectral line-shapes and stronger field enhancements can be obtained in Fano resonances [7], [8]. These characteristics show tremendous potential in a lot of fields such as sensors [9]–[14], switches [15]–[17] and slow-light devices [18]–[20]. Consequently, various plasmonic structures have been widely designed to achieve Fano resonances, especially for metal-insulator-metal (MIM) waveguides owing to the characteristics of compact footprint, deep light confinement, and compatible with fiber [21]–[27]. Over the recent past, Fano resonances based on MIM waveguides have received numerous interests due to high refractive-index sensitivities and high figure of merits (FOMs). For example, Fano

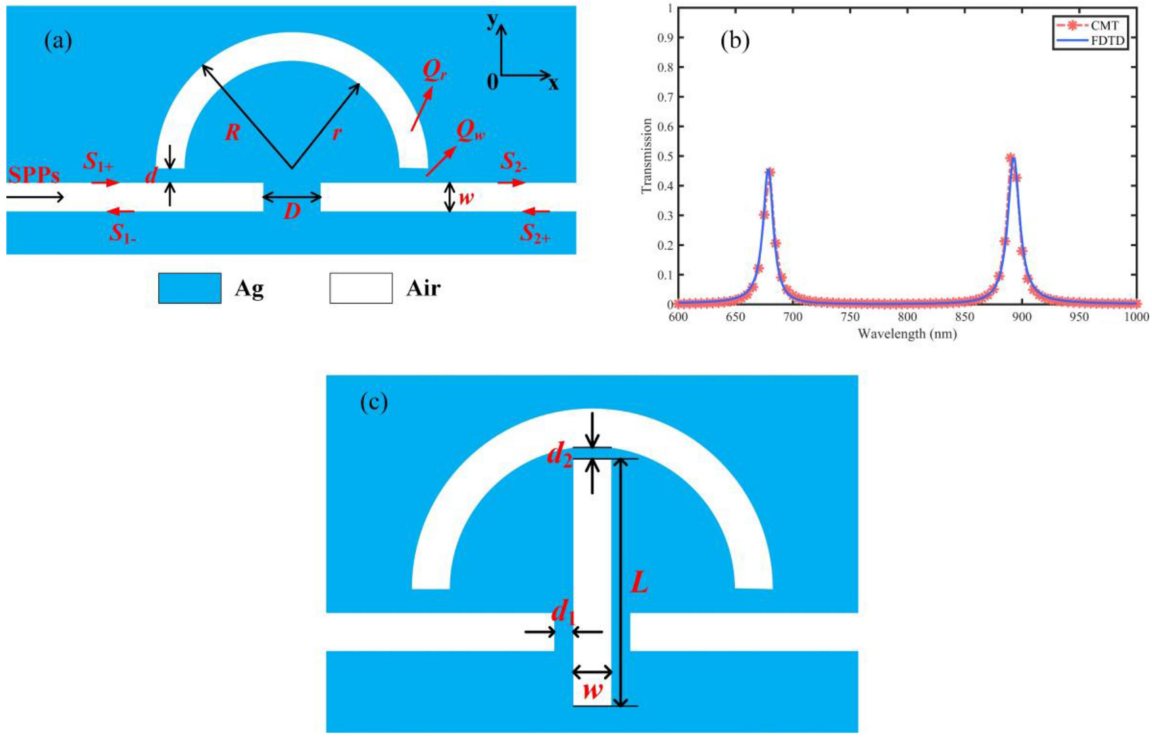

Fig. 1. (a) the scheme diagram of waveguide coupled with the semi-ring resonator, (b) transmission spectra based on FDTD and CMT methods, (c) SRRCC system consist of SRC structure and vertical rectangular groove.

resonance is achieved in MIM waveguides coupled with rectangular and ring resonators, and the sensitivity of the proposed structure can reach 1125 nm/RIU, which can be applied in sensing area [28]. Nevertheless, in order to develop highly integrated photonic circuits, multiple Fano resonant structures attract more attention than single Fano resonance in simple MIM structures. Therefore, a high tide of research on the composite conformations based on MIM waveguides is raised. In the previous work, an MIM waveguide coupled with tangent-ring resonators is proposed to achieve multiple Fano resonances [29]. Moreover, dual, triple, and quad Fano resonances with high FOMs are also realized by adding end-coupled slot cavities in the waveguide [30].

In this paper, a semi-ring-rectangular composite cavity (SRRCC) structure is investigated based on MIM waveguide. A semi-ring cavity (SRC), which is set above the input and output MIM ports, is regarded as a FP resonator. After adding a vertical rectangular cavity into the SRC system, multiple Fano resonances with high refractive index sensitivities and FOMs are achieved owing to the mode interactions, and the corresponding phase shifts and delay time within the Fano resonant windows are also investigated. Besides, through adding a new semi-ring cavity into SRRCC structure, another two Fano resonances can be obtained. Based on the characteristics explored by the finite-difference time-domain (FDTD) method and the multiple interference coupled mode theory (MICMT) method, these devices have great potential in highly integrated photonic devices

2. Simulations and Analyses

Firstly, an MIM waveguide coupled with an SRC is analyzed, and the schematic diagram is shown in Fig. 1(a). The semi-ring resonator is set above the waveguide with a coupling distance of d, and the inner and outer radii are set as r and R, respectively. The distance between the input and output ports is set as D, and the widths of both input and output ports are w.The insulator is air

($\varepsilon_0 = 1.0$) and the metal is silver with dielectric constant ε_m explained by the Drude model [31]: $\varepsilon_m = \varepsilon_\infty - \omega_p^2/(\omega^2 + i\omega\gamma)$, where ε_∞= 3.7, ω_p = 9.1eV and γ = 0.018eV. According to the equation of the accumulated phase shift per round trip: $\Phi = 2\varphi + 4\pi n_{eff} C/\lambda$, interference appears as Φ is equal to $2N\pi$, and the wavelength of the resonant mode is $\lambda = 2n_{eff} C/(N - 2\varphi/\pi)$, where C is the length of resonators, φ represents the phase shift brought by the reflection in the plasmonic system, and n_{eff} represents the effective index of the MIM waveguide [31].

For investigating the structure, 2D FDTD simulation is employed. In the following simulation, the parameters of the structure are $d = 50$ nm, $D = 70$ nm, $w = 50$ nm, $R = 310$ nm and $r = 260$ nm, and all of them are fixed throughout this paper. The transmission spectrum is shown in Fig. 1(b) plotted by blue solid line. Obviously, there are two FP resonant peaks emerging at ~891.956 nm and ~678.912 nm, respectively. Because of the high transmittance (>0.45) and the symmetrical line shapes, the structure can be applied in the filtering area. Furthermore, the corresponding transmission spectrum of the system is also analyzed by CMT method [32]–[34]. Based on CMT method, the transmission T of the structure can be expressed as $T = |(\frac{1}{Q_w})/(j2\delta + \frac{1}{Q_w} + \frac{1}{Q_r})|^2$, where Q_w and Q_r are the quality factors related to the coupling loss from the semi-ring resonator to the MIM waveguide and the inherent loss within the semi-ring resonator, respectively. As shown in Fig. 1(b), the transmission spectrum plotted with red-star line by CMT method matches well with the simulation results.

Subsequently, a vertical rectangular groove is added between the input and output port, with a width of w, a length of L, and a coupling distance of d_1 to the input/output port. The coupling distance between the semi-ring resonator and the groove is d_2, as shown in Fig. 1(c). In MIM waveguide, the continuum state can be considered as the resonant pass band, while the discrete state is considered as the forbidden one. Each slot cavity can provide multiple resonant modes that act as the continuum states or the discrete ones, which are depended on the location of the slot cavity (e.g., side-coupled or end-coupled to the MIM waveguide). Thus, the discrete state can be obtained in SRC system. After adding the end-coupled rectangular cavity, the pass bands are generated, which are regarded as the continuum state. Since multiple FP resonant modes are generated inside both cavities, mode interactions then occur to obtain Fano resonances with asymmetrical line shapes. In view of the coupled phases and modulus in this SRRCC system, multiple interference coupled mode theory (MICMT) [35], [36] based on CMT method is further derived to obtain a more accurate spectral response, and it can be given as follows:

$$\begin{cases} \frac{da_n}{dt} = -(j\omega_n + \frac{1}{t_{n0}} + \frac{1}{t_{n1}} + \frac{1}{t_{n2}})a_n + \eta_{n1} S_{n,1+} + \eta_{n2} S_{n,2+} \\ S_{1-} = -S_{1+} + \sum_n \eta_{n1}^* a_n, \quad S_{2-} = -S_{2+} + \sum_n \eta_{n2}^* a_n \\ S_{n,1+} = \gamma_{n1} e^{j\phi_{n1}} S_{1+}, \quad S_{n,2+} = \gamma_{n2} e^{j\phi_{n2}} S_{2+} \\ \eta_{n1} = \sqrt{\frac{2}{t_{n1}}} e^{j\theta_{n1}}, \quad \eta_{n2} = \sqrt{\frac{2}{t_{n2}}} e^{j(\theta_{n2} - \psi_n)} \end{cases}, \tag{1}$$

where a_n and ω_n represent the field amplitude and resonant frequency of the n-th resonant mode, respectively. t_{n0} is set as the decay time of internal loss of the n-th resonant mode. t_{n1} and t_{n2} are the decay time of the coupling between the resonator and input/output ports, respectively. $\gamma_{n1} e^{j\phi_{n1}}$ and $\gamma_{n2} e^{j\phi_{n2}}$ represent the normalized coefficients ($\gamma_{n1} = \gamma_{n1} \approx 1$ in the paper), ψ_n is the phase difference of the n-th resonant mode between input and output ports. θ_{n1} and θ_{n2} are the coupling phases of the n-th resonant mode. Since SPP is only launched from the left side into the structure, S_{2+} can be assumed to be $S_{2+} = 0$, so the complex amplitude transmission coefficient can be expressed as:

$$t_n = \frac{S_{2-}}{S_{1+}} = \sum_n \frac{\gamma_{n1} |\eta_{n1}| |\eta_{n2}| e^{j\phi_n}}{-j(\omega - \omega_n) + \frac{1}{t_{n0}} + \frac{1}{t_{n1}} + \frac{1}{t_{n2}}}, \tag{2}$$

where $n = 1, 2, 3, \cdots$ is the integer order of Fano resonant mode, the total coupling phase difference of the n-th resonant mode is $\phi_n = \phi_{n1} + \psi_n + \theta_{n1} - \theta_{n2}$. In the structure, the widths of both input and output ports are equal, $\theta_{n1} = \theta_{n2}$ and $t_{n0} = t_{n1} = t_{n2}$, so that the equation of transmittance

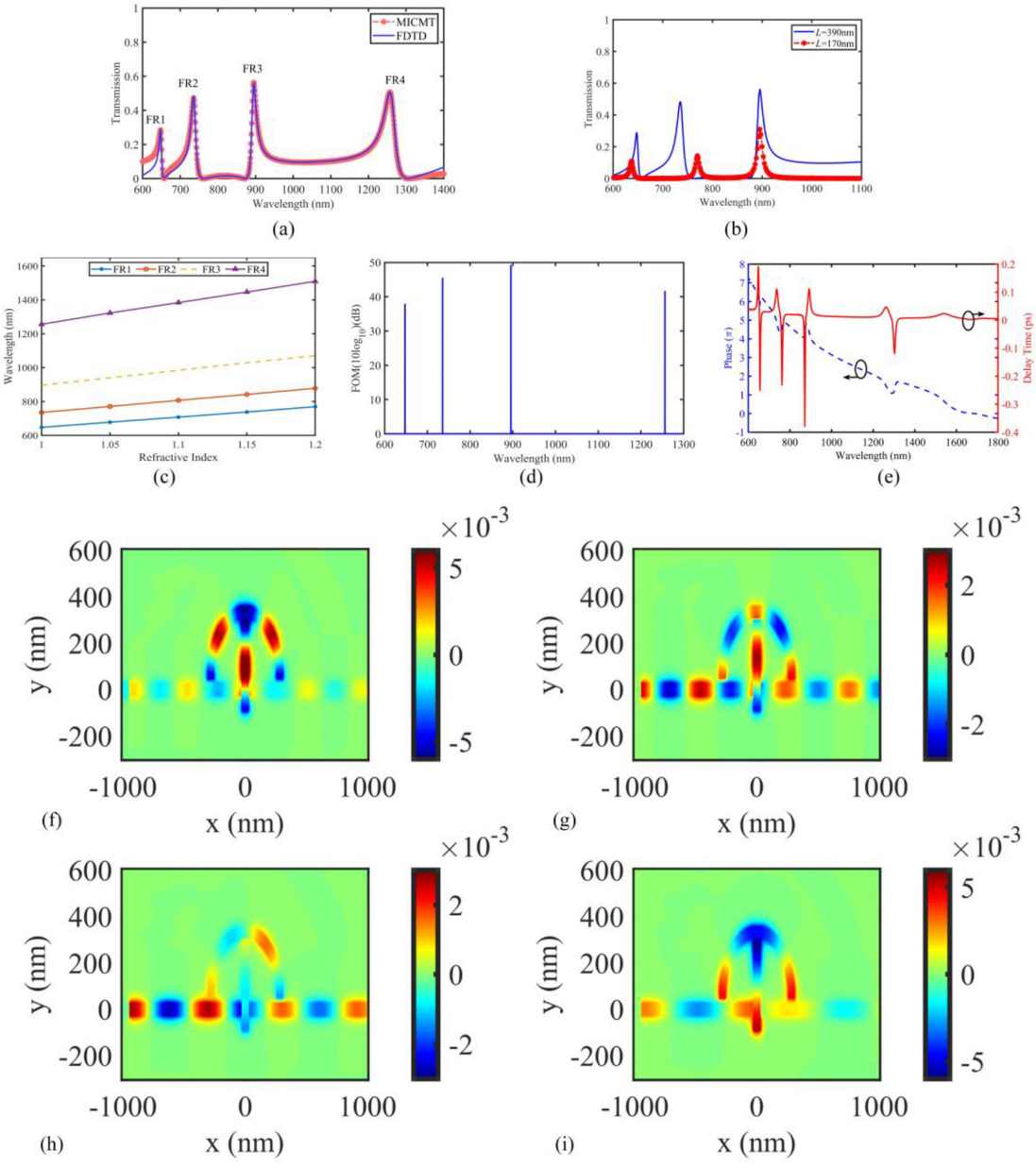

Fig. 2. (a) transmission spectra based on FDTD and MICMT methods, (b) transmission spectrum when $L = 390$ nm and $L = 170$ nm, (c) the sensitivities of FR1, FR2, FR3 and FR4, respectively, (d) FOMs of FR1, FR2, FR3 and FR4, respectively, (e) the group delays and phase responses of the SRRCC structure, and (f)–(i) are the magnetic fields of the peaks of FR1, FR2, FR3 and FR4, respectively.

can be simplified as:

$$T = \left| \sum_n \frac{2\gamma_{n1} e^{j\phi_n}}{-j(\omega - \omega_n)t_n + 2 + \frac{t_n}{t_{n0}}} \right|^2, \phi_n = \phi_{n1} + \psi_n. \tag{3}$$

In FDTD simulation, the parameters of the rectangular cavity are set as: $w = 50$ nm, $L = 390$ nm, and $d_1 = d_2 = 10$ nm. As the transmission spectrum shown in Fig. 2(a), there are four asymmetrical ultra-sharp Fano resonant peaks (i.e., four resonant modes), which are represented as FR1, FR2,

FR3 and FR4, respectively. The corresponding transmittances and the wavelengths for four Fano peaks are ∼0.289 at ∼647.585 nm, ∼0.483 at ∼735.672 nm, ∼0.562 at ∼895.513 nm and ∼0.507 at ∼1256.22 nm, respectively. The complex amplitude transmission coefficient of the other resonant modes is assumed as t_0, thus the transmission coefficient can be expressed as $t = t_0 + t_1 + t_2 + t_3 + t_4$. The transmission spectrum obtained by MICMT method is also plotted with red-star line in Fig. 2(a), which is almost identical with the FDTD simulation result. In addition, electromagnetically induced transparency (EIT) has been confirmed by scientists to be a special phenomenon of Fano resonance [37], [38]. As shown in Fig. 2(b) by setting $L = 170$ nm,EIT is achieved at $\lambda = \sim 769.534$ nm, which is previously the forbidden band in Fig. 1(b), indicating that EIT is a special case of Fano resonance. Therefore, the proposed structure can be applied in the sensing area. In order to evaluate the sensing characteristics of the structure, the sensitivity, one of the most important factors, is expressed as [39]:

$$S = \frac{d\lambda}{dn(\lambda)}, \tag{4}$$

where λ and $n(\lambda)$ represent the resonant wavelength and the refractive index of the resonator, respectively. When $n(\lambda)$ increases from 1.0 to 1.2 with a step of 0.05, the wavelength variations of Fano resonant peaks are shown in Fig. 2(c). According to Eq. (4), it can be calculated that sensitivities of FR1, FR2, FR3 and FR4 are ∼608.64 nm/RIU, ∼711.14 nm/RIU, ∼876.88 nm/RIU and ∼1260.5 nm/RIU, respectively. Compared to conventional structure, Fano resonances are easier to be detected owing to their narrow bandwidths and the ultra-sharp asymmetric peaks and dips. Additionally, FOM is another factor to evaluate the performance of this structure, and it is expressed as [40]:

$$\text{FOM} = 10\log_{10}\left(\left|\frac{dT(\lambda)/dn(\lambda)}{T(\lambda)}\right|\right), \tag{5}$$

where $T(\lambda)$ is the transmission, and $dT(\lambda)/dn(\lambda)$ represents the change of transmittance caused by different refractive indexes. In accordance with the transmission spectrum in Fig. 2(a) and Eq. (5), the maximum FOM values corresponding to Fano resonances can be calculated as ∼37.94 dB, ∼45.56 dB, ∼49.24 dB, and ∼41.67 dB, respectively, as shown in Fig. 2(d).

Furthermore, group delays τ and phase responses θ are also studied. According to the expression of the phase response and delay time: $\tau(\lambda) = -\frac{\lambda^2}{2\pi c}\frac{d\theta}{d\lambda}$ [41], their variations with respect to the wavelength are plotted in the Fig. 2(e), where the red line and the blue line represent the phase response and the delay time, respectively. Obviously, phase shifts will occur within all the Fano resonant windows, leading to negative and positive time delays around the dips and peaks, respectively. For the dips, the largest delay values are ∼−0.217 ps, ∼−0.202 ps, ∼−0.326 ps and ∼−0.098 ps achieved at ∼657 nm, ∼763 nm, ∼871 nm and ∼1304 nm, respectively. On the contrary, positive delays with maximum values of ∼0.167 ps, ∼0.0955 ps, ∼0.0958 ps, ∼0.0389 ps are obtained at the Fano-peak wavelengths. The magnetic field distributions corresponding to the peaks of FR1, FR2, FR3 and FR4 are shown in Figs. 2(f)–(i), in which the SPPs propagation details for the resonant peaks can be observed. The normal and abnormal dispersion can be obtained in this proposed structure. Therefore, the system benefitted from the group delays can be well applied in the fast or slow light technologies., which are preferred in optical buffer and storage [42]–[44].

Next, according to the research above, a dual-semi-ring rectangular composite cavity (DSRRCC) structure, which consists of a new concentric semi-ring with an inner radius of r_1 and an outer radius of R_1 in the SRRCC system, is proposed and shown in Fig. 3(a). During FDTD simulation, the inner and outer radii are $r_1 = 360$ nm and $R_1 = 430$ nm, respectively, and the transmission spectrum is shown in Fig. 3(b). Compared with the SRRCC system, there are two new Fano peaks, one (named as NFR1) appears at wavelength of ∼691.455 nm with a transmittance of ∼0.45, and the other called NFR2 arises at ∼1121.35 nm with a transmittance of ∼0.59, respectively.

According to Eqs. (4) and (5), the sensitivities and the maximum FOMs can be obtained, as shown in Figs. 3(c) and (d), respectively. For NFR1, the sensitivity is ∼663.594 nm/RIU and

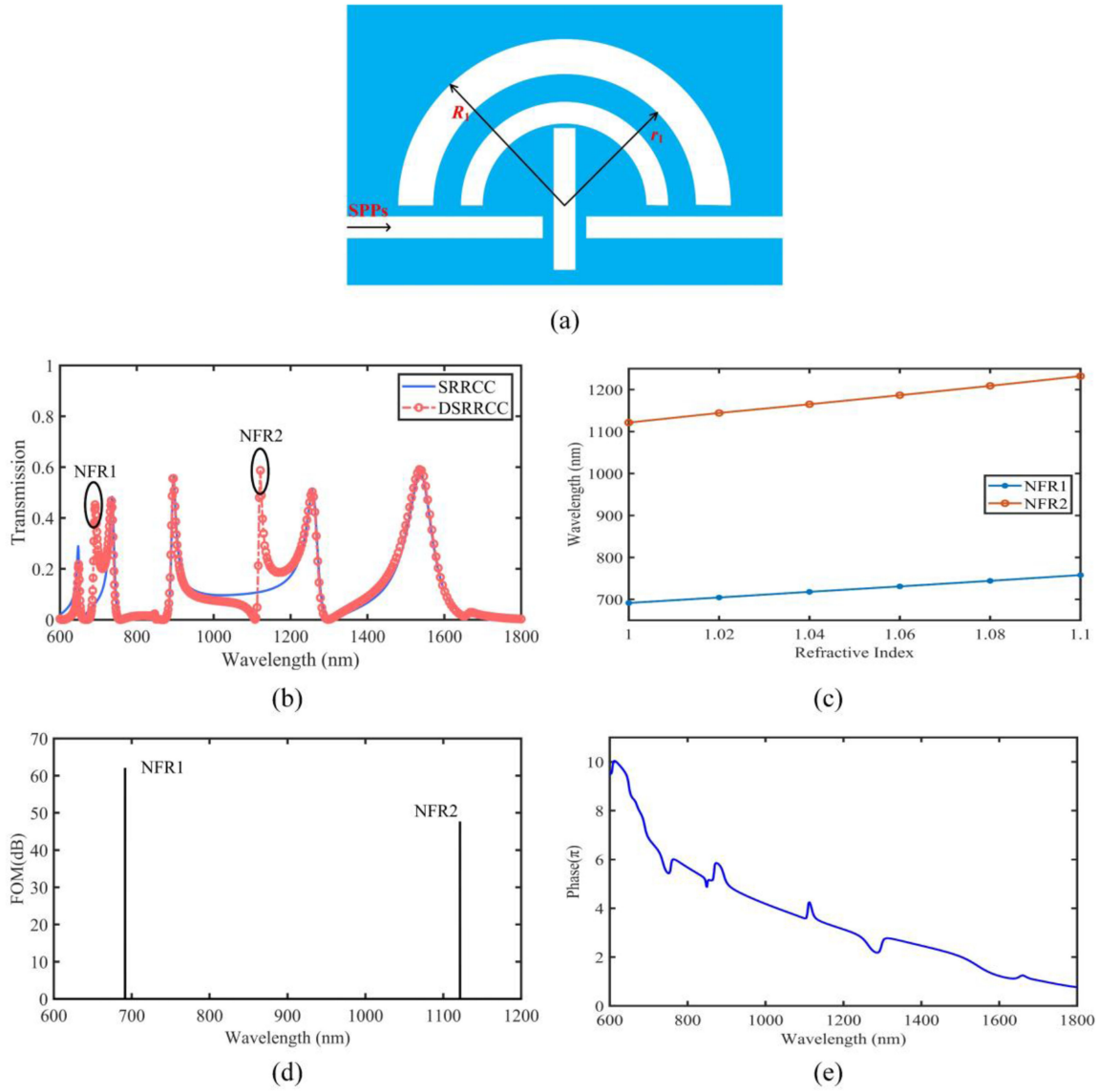

Fig. 3. (a) the scheme diagram of DSRRCC structure consisting of SRRCC structure and a new semi-ring cavity, (b) transmission spectra of the SRRCC and DSRRCC based on FDTD method, (c) the sensitivities of NFR1 and NFR2, respectively, (d) the FOMs of NFR1 and NFR2, respectively, and (e) is the phase response of DSRRCC system.

FOM is ∼62.08 dB, while the sensitivity and FOM of NFR2 are ∼1099.1 nm/RIU and ∼47.67 dB, respectively. The phase response with respect to the wavelength is also analyzed. As shown in Fig. 3(e), phase shifts are also achieved around the NFR1 and NFR2 windows. Therefore, Fano resonances can be increased in the DSRRCC system, which has more potential in the integrated photonic circuits.

3. Conclusions

In summary, there are four Fano resonances in the proposed SRRCC structure, which has been investigated by using FDTD and MICMT methods. Through numerically calculation, high sensitivities

of ∼608.64 nm/RIU, ∼711.14 nm/RIU, ∼876.88 nm/RIU and ∼1260.5 nm/RIU, and high FOMs of ∼37.94 dB, ∼45.56 dB, ∼49.24 dB and ∼41.67 dB can be obtained for four peaks, which show great potential in the sensing areas. Additionally, the SRRCC system can be utilized in slow/fast-light device because of the negative or positive delay time around the dips or peaks, respectively. Nevertheless, two more Fano resonances arise based on DSRRCC structure with high sensitivities and FOMs. It is believed that these proposed structures can find important applications in highly integrated on-chip sensing devices.

Acknowledgment

The authors would like to thank the editors and reviewers for their valuable comments and suggestions, which have greatly improved the quality of the manuscript. The authors also would like to thank for Prof. Yuwen Qin's and Prof. Yi Dong's help to revise the manuscript.

References

[1] M. F. Limonov, M. V. Rybin, A. N. Poddubny, and Y. S. Kivshar, "Fano resonances in photonics," *Nature Photon.*, vol. 11, no. 9, pp. 543–554, 2017.
[2] U. Fano, "Effects of configuration interaction on intensities and phase shifts," *Phys. Rev.*, vol. 124, no. 6, 1961, Art. no. 1866.
[3] B. Luk'yanchuk *et al.*, "The Fano resonance in plasmonic nanostructures and metamaterials," *Nature Mater.*, vol. 9, no. 9, pp. 707–715, 2010.
[4] R. Guo *et al.*, "Plasmonic fano nanoantennas for on-chip separation of wavelength-encoded optical signals," *Nano Lett.*, vol. 15, no. 5, pp. 3324–3328, 2015.
[5] W. F. Zhang, W. Z. Li, and J. P. Yao, "Optically tunable Fano resonance in a gratingbased Fabry–Perot cavity-coupled microring resonator on a silicon chip," *Opt. Lett.*, vol. 41, no. 11, pp. 2474–2477, 2016.
[6] A. Li and W. Bogaerts, "An actively controlled silicon ring resonator with a fully tunable Fano resonance," *APL Photon.*, vol. 2, no. 9, 2017, Art. no. 096101.
[7] B. Gallinet and O. J. Martin, "Influence of electromagnetic interactions on the line shape of plasmonic Fano resonances," *ACS Nano*, vol. 5, no. 11, pp. 8999–9008, 2011.
[8] E. Miroshnichenko, B. A. Malomed, and Y. S. Kivshar, "Nonlinearly PT-symmetric systems: Spontaneous symmetry breaking and transmission resonances," *Phys. Rev. A.*, vol. 84, no. 1, 2011, Art. no. 012123.
[9] T. Weiss, M. Mesch, M. Schäferling, H. Giessen, W. Langbein, and E. A. Muljarov, "From dark to bright: First-order perturbation theory with analytical mode normalization for plasmonic nanoantenna arrays applied to refractive index sensing," *Phys. Rev. Lett.*, vol. 116, no. 23, 2016, Art. no. 237401.
[10] J. Ye *et al.*, "Plasmonic nanoclusters: Near field properties of the Fano resonance interrogated with SERS," *Nano Lett.*, vol. 12, no. 3, pp. 1660–1667, 2012.
[11] J. Chen, Z. Li, J. Li, and Q. Gong, "Compact and high-resolution plasmonic wavelength demultiplexers based on Fano interference," *Opt. Exp.*, vol. 19, no. 10, pp. 9976–9985, 2011.
[12] S. Roh, T. Chung, and B. Lee, "Overview of the characteristics of micro-and nano-structured surface plasmon resonance sensors," *Sensors*, vol. 11, no. 2, pp. 1565–1588, 2011.
[13] W. Lai, K. Wen, J. Lin, Z. Guo, Q. Hu, and Y. Fang, "Plasmonic filter and sensor based on a subwavelength end-coupled hexagonal resonator," *Appl. Opt.*, vol. 57, no. 22, pp. 6369–6374, 2018.
[14] S. Zhan *et al.*, "Tunable nanoplasmonic sensor based on the asymmetric degree of Fano resonance in MDM waveguide," *Sci. Rep., UK*, vol. 6, 2016, Art. no. 22428.
[15] H. Lu, X. Liu, L. Wang, Y. Gong, and D. Mao, "Ultrafast all-optical switching in nanoplasmonic waveguide with Kerr nonlinear resonator," *Opt. Exp.*, vol. 19, no. 4, pp. 2910–2915, 2011.
[16] K. Nozaki, A. Shinya, S. Matsuo, T. Sato, E. Kuramochi, and M. Notomi, "Ultralow-energy and high-contrast all-optical switch involving Fano resonance based on coupled photonic crystal nanocavities," *Opt. Exp.*, vol. 21, no. 10, pp. 11877–11888, 2013.
[17] W. S. Chang *et al.*, "A plasmonic Fano switch," *Nano Lett.*, vol. 12, no. 9, pp. 4977–4982, 2012.
[18] N. Verellen *et al.*, "Fano resonances in individual coherent plasmonic nanocavities," *Nano Lett.*, vol. 9, no. 4, pp. 1663–1667, 2009.
[19] R. Zafar and M. Salim, "Wideband slow light achievement in MIM plasmonic waveguide by controlling Fano resonance," *Infrared Phys. Technol.*, vol. 67, pp. 25–29, 2014.
[20] B. Yun, G. Hu, R. Zhang, and Y. Cui, "Fano resonances in a plasmonic waveguide system composed of stub coupled with a square cavity resonator," *J. Opt., UK*, vol. 18, no. 5, 2016, Art. no. 055002.
[21] J. Qi *et al.*, "Independently tunable double Fano resonances in asymmetric MIM waveguide structure," *Opt. Exp.*, vol. 22, no. 12, pp. 14688–14695, 2014.
[22] H. Lu, X. Liu, D. Mao, and G. Wang, "Plasmonic nanosensor based on Fano resonance in waveguide-coupled resonators," *Opt. Lett.*, vol. 37, no. 18, pp. 3780–3782, 2012.
[23] K. Wen, Y. Hu, L. Chen, J. Zhou, L. Lei, and Z. Guo, "Fano resonance with ultra-high figure of merits based on plasmonic metal-insulator-metal waveguide," *Plasmonics*, vol. 10, no. 1, pp. 27–32, 2015.

[24] Z. Chen, L. Yu, L. Wang, G. Duan, Y. Zhao, and J. Xiao, "A refractive index nanosensor based on Fano resonance in the plasmonic waveguide system," *IEEE Photon. Technol. Lett.*, vol. 27, no. 16, pp. 1695–1698, Aug. 2015.
[25] X. Zhao, Z. Zhang, and S. Yan, "Tunable Fano resonance in asymmetric MIM waveguide structure," *Sensors*, vol. 17, no. 7, 2017, Art. no. 1494.
[26] X. Shen, Y. Wang, X. Yan, L. Yuan, and T. Sang, "Transmission characteristics and transmission line model of a metal-insulator-metal waveguide with a stub modified by cuts," *Appl. Opt.*, vol. 55, no. 23, pp. 6443–6446, 2016.
[27] D. Ding, M. J. A. de Dood, J. F. Bauters, M. J. Heck, J. E. Bowers, and D. Bouwmeester, "Fano resonances in a multimode waveguide coupled to a high-Q silicon nitride ring resonator," *Opt. Exp.*, vol. 22, no. 6, pp. 6778–6790, 2014.
[28] Y. Tang *et al.*, "Refractive index sensor based on Fano resonances in metal-insulator-metal waveguides coupled with resonators," *Sensors*, vol. 17, no. 4, 2017, Art. no. 784.
[29] Z. Guo, K. Wen, Q. Hu, W. Lai, J. Lin, and Y. Fang, "Plasmonic multichannel refractive index sensor based on subwavelength tangent-ring metal–insulator–metal waveguide," *Sensors, Basel*, vol. 18, no. 5, 2018, Art. no. 1348.
[30] K. Wen, L. Chen, J. Zhou, L. Lei, and Y. Fang, "A plasmonic chip-scale refractive index sensor design based on multiple Fano resonances," *Sensors*, vol. 18, no. 10, 2018, Art. no. 3181.
[31] Z. Chen, J. Chen, L. Yu, and J. Xiao, "Sharp trapped resonances by exciting the anti-symmetric waveguide mode in a metal-insulator-metal resonator," *Plasmonics*, vol. 10, no. 1, pp. 131–137, 2015.
[32] H. A. Haus and W. Huang, "Coupled-mode theory," *Proc. IEEE*, vol. 79, no. 10, pp. 1505–1518, Oct. 1991.
[33] Q. Li, T. Wang, Y. Su, M. Yan, and M. Qiu, "Coupled mode theory analysis of mode-splitting in coupled cavity system," *Opt. Exp.*, vol. 18, no. 8, pp. 8367–8382, 2010.
[34] K. Wen, Y. Hu, J. Zhou, L. Lei, J. Li, and Y. Wu, "Plasmonic-induced absorption in an end-coupled metal-insulator-metal resonator structure," *Opt. Mater. Exp.*, vol. 7, no. 2, pp. 433–443, 2017.
[35] S. Li, Y. Wang, R. Jiao, L. Wang, G. Duan, and L. Yu, "Fano resonances based on multimode and degenerate mode interference in plasmonic resonator system," *Opt. Exp.*, vol. 25, no. 4, pp. 3525–3533, 2017.
[36] H. Fu *et al.*, "Independently tunable ultrasharp double fano resonances in coupled plasmonic resonator system," *IEEE Photon. J.*, vol. 10, no. 1, Feb. 2018, Art. no. 4800409.
[37] W. F. Zhang, W. Z. Li, and J. P. Yao, "Optically tunable Fano resonance in a grating-based Fabry–Perot cavity-coupled microring resonator on a silicon chip," *Opt. Lett.*, vol. 41, no. 11, pp. 2474–2477, 2016.
[38] G. C. Wang *et al.*, "Fano-resonance-based ultra-high-resolution ratio-metric wavelength monitor on silicon," *Opt. Lett.*, vol. 41, no. 3, pp. 544–547, 2016.
[39] N. Liu, M. Mesch, T. Weiss, M. Hentschel, and H. Giessen, "Infrared perfect absorber and its application as plasmonic sensor," *Nano Lett.*, vol. 10, no. 7, pp. 2342–2348, 2010.
[40] J. Becker, A. Trügler, A. Jakab, U. Hohenester, and C. Sönnichsen, "The optimal aspect ratio of gold nanorods for plasmonic bio-sensing," *Plasmonics*, vol. 5, no. 2, pp. 161–167, 2010.
[41] K. Wen *et al.*, "Plasmonic-induced absorption and transparency based on a compact ring-groove joint MIM waveguide structure," *IEEE Photon. J.*, vol. 8, no. 5, Oct. 2016, Art. no. 4802308.
[42] C. J. Chang-Hasnain, P. C. Ku, J. Kim, and S. L. Chuang, "Variable optical buffer using slow light in semiconductor nanostructures," *Proc. IEEE*, vol. 91, no. 11, pp. 1884–1897, Nov. 2003.
[43] T. F. Krauss, "Why do we need slow light?" *Nature Photon.*, vol. 2, no. 8, pp. 448–450, 2008.
[44] L. Thévenaz, "Slow and fast light in optical fibres," *Nature Photon.*, vol. 2, no. 8, pp. 474–481, 2008.